Available online at www.sciencedirect.com
ScienceDirect
Journal of Colloid and Interface Science 306 (2007) 56–65
JOURNAL OF Colloid and Interface Science
www.elsevier.com/locate/jcis

Electrochemical formation of crooked gold nanorods and gold networked structures by the additive organic solvent

Chien-Jung Huang [a,*], Pin-Hsiang Chiu [b], Yeong-Her Wang [b,c], Cheng-Fu Yang [d], Shih-Wei Feng [a]

[a] *Department of Applied Physics, National University of Kaohsiung, #700 Kaohsiung University Rd., Nan-Tzu, Kaohsiung, Taiwan*
[b] *Institute of Electro-Optical Science and Engineering, National Cheng-Kung University, #1 University Rd., Tainan, Taiwan*
[c] *Institute of Microelectronics, Department of Electrical Engineering, National Cheng-Kung University, #1 University Rd., Tainan, Taiwan*
[d] *Department of Chemical and Materials Engineering, National University of Kaohsiung, #700 Kaohsiung University Rd., Nan-Tzu, Kaohsiung, Taiwan*

Received 31 July 2006; accepted 2 October 2006

Available online 6 October 2006

Abstract

Crooked gold nanorods (CGNRs) and gold network structures are fabricated using a simple electrochemical approach. The growth solution is prepared by surfactant solution as micelle templates with isopropanol (IPA) solvent. The shape of crooked nanorods and networks structure depend on the amount of added IPA solvent. To investigate the influence of isopropanol solvent on the CGNRs, the amount of IPA was varied in the range from 0.05 to 0.2 mL. It was found that the aspect ratios (γ) of CGNRs were in the range from 1.06 to 1.46, and the UV–vis absorption measurement revealed a pronounced red-shift of the surface plasmon resonance (SPR) band from 532 to 560 nm. High-resolution transmission electron microscopy (HRTEM) showed that the formation of crooked nanorod structure was induced by aggregation of many small gold nuclei between the several large gold nanoparticles during growth, causing the small gold nuclei to link the gold nanoparticles. The CGNRs have a polycrystalline structure via the analysis from selected-area electron diffraction (SAED).

Keywords: Gold; Nanoparticles; Nanorods; Surfactant; Micelle; Electrochemical

1. Introduction

Synthesis of gold nanoparticles with a specific size and morphology has recently attracted a lot of interest due to their fundamental importance and potential application in various fields, thus highlighting the significance of developing a special shape and structure for gold nanoparticles. Hence, controlling the shape and structure during nanoparticle synthesis is an emerging research topic. Several synthetic methods of preparing metallic nanorods exist, such as electrochemical synthesis in solution [1], electrochemical deposition in hard templates [2], solution-phase method based on capping reagents [3], photochemical synthesis [4], wet chemical synthesis based on a seed-mediated growth mechanism [5] and microwave heating [6].

The organization and growth of nanoparticles into nanowires with a networked structure have been widely studied recently. For example, Schmid et al. have reported the two-dimensional (2D) networks via quasi one-dimensional (1D) arrangements of gold clusters [7]. Kondow et al. studied the formation of gold nanonetworks by irradiation of intense pulsed laser on gold nanoparticles [8]. Wang et al. created networked gold nanostructures and twisted gold nanorods in water by laser ablation technique [9]. Chang et al. observed that silver nanoparticles spontaneously organized themselves into nanobanners structures in supercritical water [10]. Pileni et al. prepared the copper network structures in sodium dodecyl sulfate solution by reducing copper dodecyl sulfate [11]. Thus, special nanoarchitectures such as snowflakes, dandelions, dendrimer-like structures and nanoflowers have recently been reported [12–15]. It is believed that these special nanomaterials have marvelous ability to control optical properties. Therefore, investigation of simple synthesis approaches for 1D or 2D nanomaterials with well-

* Corresponding author. Fax: +886 7 5919357.
E-mail address: chien@nuk.edu.tw (C.-J. Huang).

0021-9797/$ – see front matter
doi:10.1016/j.jcis.2006.10.009

defined structures and unique properties has been drawn more and more efforts for both academic purpose and potential applications.

The production of metal nanoparticles via an electrochemical method has been widely researched since the early research by Reetz [16]. Electrochemistry has not been employed as a means of preparing large numbers of metal nanoparticles, but some advantages of electrochemical methods over chemical ones in synthesis of small metal particles are the high purity of the particles and the possibility of a precise particle size controlled by adjusting current density or applied potential [17]. In the present study, the advantages of electrochemical method by organic IPA solvent addition are the low-processing temperature, high-growth rate, short reaction time and easy modulation shape of particle. Very recently, gold nanorods with fairly good uniformity and controlled aspect ratio have also been synthesized via this electrochemical method [18]. For the growth of these gold nanorods, generally, a template method with a dynamic surfactant micelle system serving as the soft template is considered to be suitable; the addition of a small amount of organic solvent to the surfactant solution is necessary for enhancing the formation of the rod-like micelle [19]. Our research group developed electrochemical method for synthesis of gold nanocubes [20,21]. Carefully controlling the amount of acetone solvent added to the surfactant solution during electrolysis changed the particle shape from sphere to cube. Therefore, the electrochemical reaction of organic solvent with surfactant solution is critical for obtaining the proper morphology of nanoparticles, but little research has been carried out on the exact role of organic solvent.

To develop this technique further, this study demonstrates a simpler electrochemical method for synthesizing 1D crooked gold nanorods (CGNRs) and 2D gold network structures in the presence of isopropanol (IPA) solvent with ionic surfactant solution. The role of IPA solvent is found to induce the CGNRs formation. Besides, the formation mechanism of the 1D crooked nanorods and 2D network structures is also proposed and discussed.

2. Experimental

2.1. Chemicals

Cationic cetyltrimethylammonium bromide ($C_{16}H_{33}(CH_3)_3N^+Br^-$; CTAB, 98%) and cationic tetradecyltrimethylammonium bromide ($C_{45}H_{91}(CH_3)_3N^+Br$; TTAB, 99%) were obtained from Fluka. Isopropanol ($CH_3CHOHCH_3$; IPA, 99%) was purchased from J.T. Baker. Reagent alcohol from Sigma, hydrochloric acid from Merck and nitric acid from Merck were employed. Aqua Regia was supplied as a mixture of hydrochloric acid and nitric acid (3:1 wt%). All chemicals were of analytical grade and were used without further purification. The water used throughout the experiments is purified by a Milli-Q system (Millipore resistivity 18.2 MΩ cm).

2.2. Electrochemical apparatus

The gold nanoparticles were synthesized in a simple two-electrode cell by using a power supply (MOTECH LPS-305, Taiwan). The actually experimental cell was housed in a standard 20 × 80 mm glass test tube. Gold and platinum plates with dimensions of 30 × 10 × 0.5 mm were cut to form, respectively, the anode and cathode. The gold and platinum plates, both 99.99% pure, were purchased from Gredmann. Before each experiment, the gold electrode was polished by hand using fine grade emery paper, and was washed with water and a small amount of acetone. The platinum electrode was washed with aqua regia to dissolve gold residue after the experiment was completed. Finally, these electrodes were blown with high-purity nitrogen gas. The two electrodes were placed vertically face-to-face inside the cell. Electrodes in the cell were spaced 5 mm apart and held in place by Teflon spacers.

2.3. Synthesis of crooked gold nanorods

In a typical synthesis, the surfactant CTAB (0.08 M) served as the electrolyte 3 mL of growth solution was placed in the glass test tube. A 30 mg amount of powdered co-surfactant TTAB was then added to the same test tube. TTAB is a rod-inducing surfactant. And then a pipette was used to add 0.2 mL of IPA solvent. The test tube was then sonicated for 5 min. The electrolysis was carried out for 25 min with an applied current of 5 mA at a temperature of 40 °C under constant ultrasonication.

2.4. Characterization

The shape and size of the samples were measured by transmission electron microscopy (TEM, JEOL JEM-1230) operating at 100 kV. The high-resolution atomic image and electron diffraction (ED) were performed on a field emission gun TEM (FEG-TEM, Philips Tecnai G2 F20), working at 200 kV accelerating voltage and equipped with an energy-dispersive X-ray spectrometric (EDS) element analyses. The formation of gold particle was confirmed by EDS analysis. The shortest dimension of CGNRs was defined as the particle size (diameter), and the longest dimension was defined as the particle length. The histograms distributions of diameter (D_i) and length (L_i) for each sample were determined by manual measurements using over 200 particles in TEM images. The standard deviation (σ) is given by the following relationship [22]:

$$\sigma = \left\{ \sum \left[N(D_i - D)^2 \right] / (N-1)^2 \right\}^{1/2},$$

$$\sigma = \left\{ \sum \left[N(L_i - L)^2 \right] / (N-1)^2 \right\}^{1/2},$$

where D and L denote the average diameter and average length, respectively, and N denotes is the number of particles.

For the observation of TEM and UV–vis, the samples were obtained by the following procedure. The resulting solution was centrifuged (Hettich MIKO-22R, Japan) at 6500 rpm for 20 min to remove excess surfactant, and the resulting supernatant gold

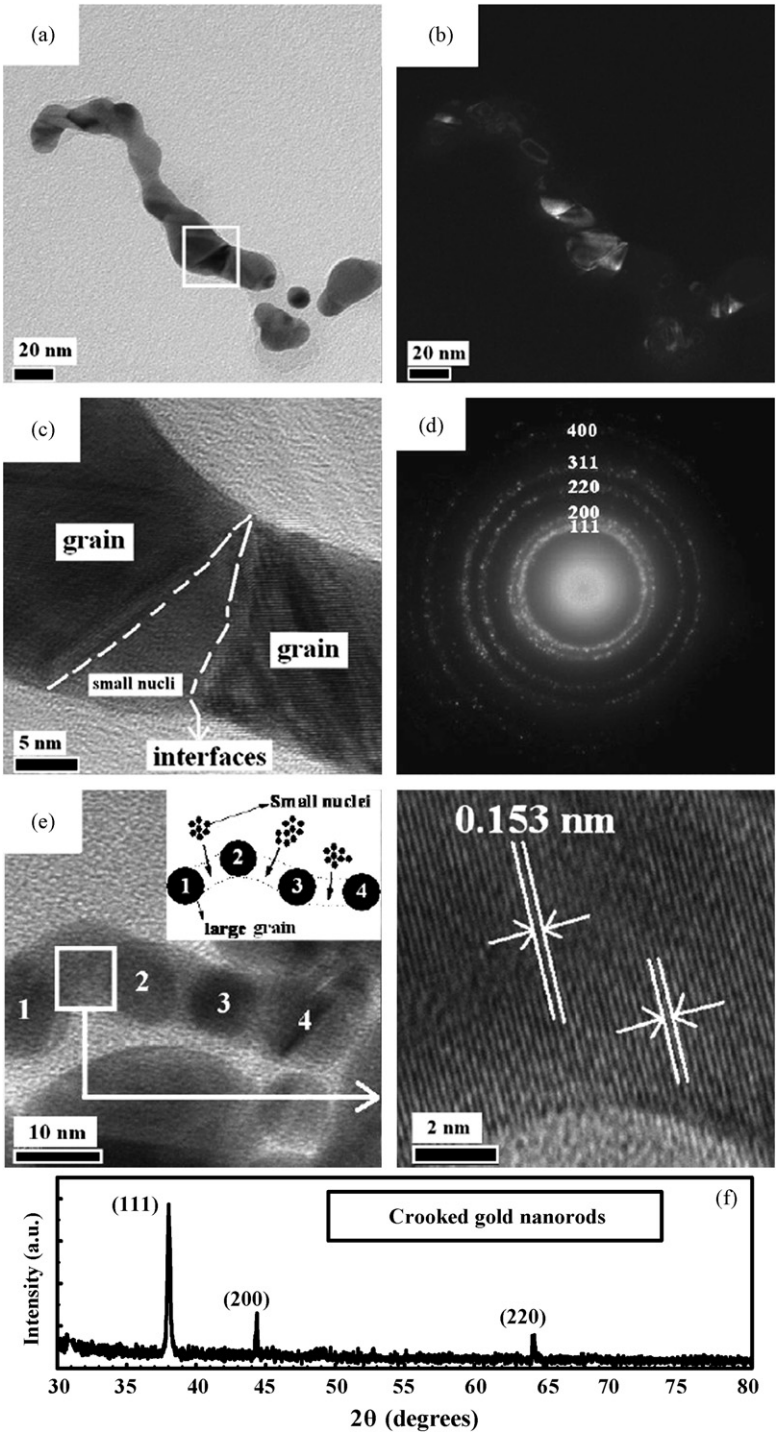

Fig. 1. TEM micrographs of crooked gold nanorods prepared with 0.2 mL IPA in (a) bright-field image and (b) dark-field image. (c) HRTEM image in a white frame in panel (a). (d) Selected-area electron diffraction pattern of (a). (e) Schematic illustration of a single crooked gold nanorod and the right HRTEM image in a white frame in panel (e). (f) XRD patterns of crooked gold nanorods deposited on quartz substrate.

colloid was divided equally into two test solutions. A centrifugation is helpful for increasing the yield of gold nanoparticles further, since it enables the gold nanoparticles to be separated from the reaction medium. The test solution was employed to measure the UV–vis absorbance by a 1.5 mL cavity sorted cuvette at room temperature. Another test solution was centrifuged again at 12000 rpm for 20 min, and then the precipitation was collected and redispersed in a small amount of water. A droplet (7 μL) of the precipitate was then placed on a standard 200-mesh 3 mm carbon-coated copper grid (Agar Scientific, England) on a filter paper and allowed to dry at room temperature (∼25 °C) in the electronic dry cabinet (Jow Ruey Technical DRY-70, Taiwan) for rapid removal of the liquid. For the X-ray diffraction (XRD) measurements, the sample was prepared by

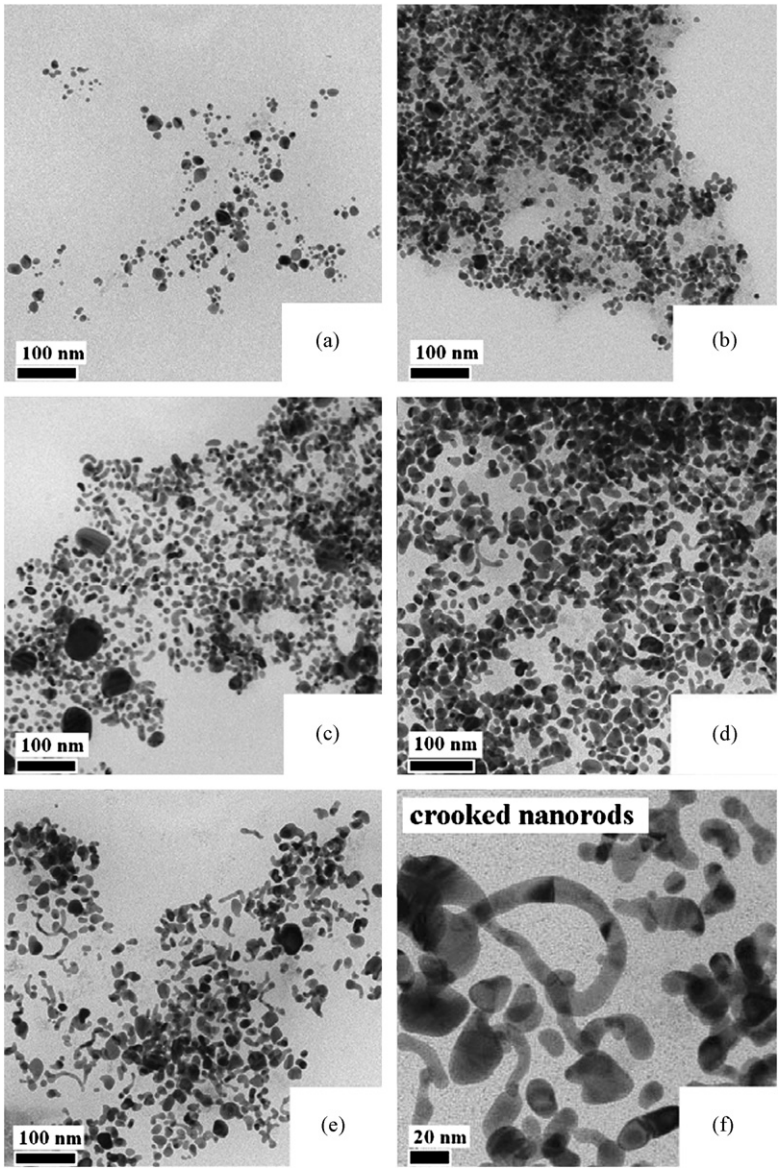

Fig. 2. TEM images of gold nanoparticles obtained by adding (a) 0, (b) 0.05, (c) 0.1, (d) 0.15, and (e) 0.2 mL IPA. (f) The expanded picture illustrates the crooked gold nanorods.

drop-casting one drop of the growth solution onto a clean quartz substrate, which was then dried in air. The sample was then examined on a MAC science (MXT-III) instrument operating at 40 kV and a current of 30 mA with Cu$K\alpha$ radiation.

3. Results and discussion

3.1. Structures of crooked gold nanorods

A typical bright-field (BF) TEM image of single CGNRs was prepared with 0.2 mL of IPA, as shown in Fig. 1a. The electron micrograph pattern reveals that CGNRs were formed with some large grains. Fig. 1b shows the dark-field (DF) TEM image of the single CGNRs, as shown in Fig. 1a. DF imaging analysis, as shown in Fig. 1b, demonstrates that this contrast arose from segments of individual grains oriented for strong Bragg scattering. Several grains exhibiting strong diffraction contrast in the DF images are simultaneously visible as small, bright regions in single CGNRs. A comparison between the BF image and the corresponding DF TEM image shows that the distribution of the gold grains is not uniform. The CGNRs were clearly composed of many gold grains, several of which were present within each of the CGNRs, indicating that they were polycrystalline. Fig. 1c shows a high-resolution transmission electron microscope (HRTEM) image of some single CGNRs with a diameter of around 15 nm. The resolved lattice fringe arrangement indicates that the crooked rods consisted of polycrystalline gold, with its distinct domains probably reflecting the size and orientation of the original particles. Hence, CGNRs were formed by aggregation of many small gold nuclei between the large grains during the growth process, indicating that small gold nuclei linked the large gold grains. Fig. 1d shows the selected-area electron diffraction (SAED) pattern of CGNRs, which clearly demonstrates that the characteristic

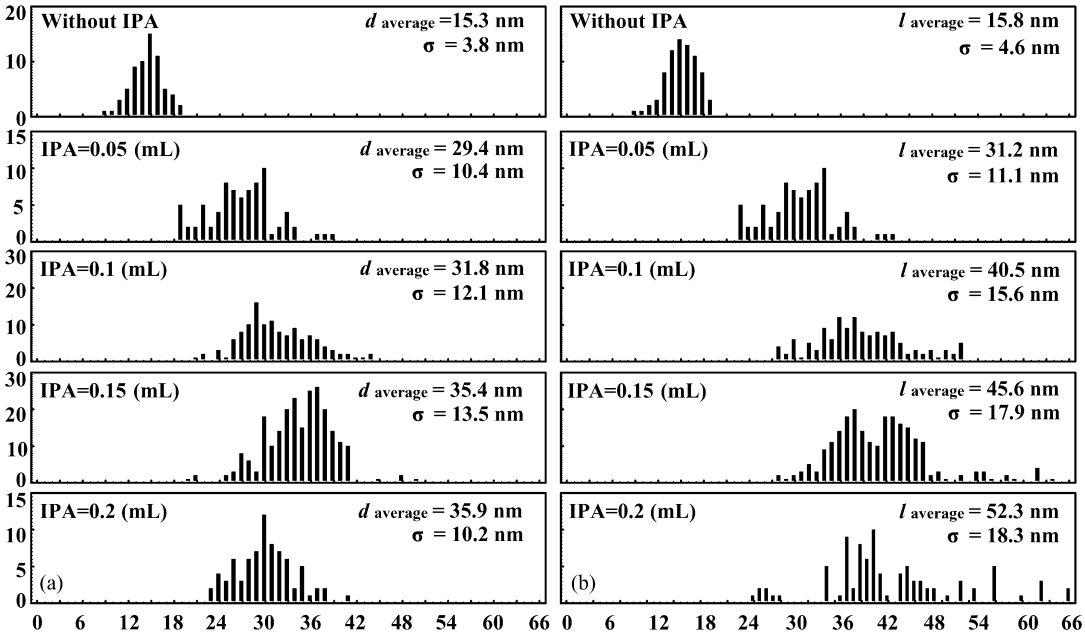

Fig. 3. Histogram of the (a) average diameter, d_{average}, and (b) average length, l_{average}, in the distribution with standard deviation, σ, of the crooked gold nanorods with of 0, 0.05, 0.1, 0.15, and 0.2 mL IPA.

ring in the polycrystalline diffraction pattern can be indexed to (111), (200), (220), (222), (311), and (400) crystalline facets, creating concentric rings with sequences corresponding to a face-centered cubic (fcc) lattice gold phase. Fig. 1e schematically shows the formation mechanism of these CGNRs by their TEM images reword, clearly showing that crooked structure consisted of four large gold particles and many small Au nuclei between the particles. This finding was further confirmed by HRTEM, as shown in the inset of Fig. 1e. The small gold nuclei linked the large gold nanoparticles. A lattice plane with a measured interplanar distance of 0.153 nm was observed. To determine the crystallographic data of the CGNRs, X-ray diffraction experiments were carried out. Fig. 1f shows the XRD patterns for CGNRs in a wide-angle range. The X-ray diffraction peaks from atomic lattices of the CGNRs clearly demonstrate that the peaks at $2\theta = 38.18°$, 44.39° and 64.57° are assigned as (111), (200) and (220) reflection lines, respectively. These peaks are consistent with the joint committee on powder diffraction standards (JCPDS 04-0784) and the earlier report [23]. No peak characteristics of any impurities were observed. The XRD pattern exhibits primarily the (111) Bragg reflection of fcc gold, indicating highly oriented growth of the crooked gold nanorods. This is a strong evidence of the preferential growth of the CGNRs along (111) directions as the particle length increases. Notably, the (200) and (220) Bragg reflections are extremely weak and considerably broadened relative to the (111) reflection, which indicates that CGNRs are highly anisotropic in shape.

3.2. Controlling the shape of crooked gold nanorods using various amount of IPA

Fig. 2 shows typical TEM images of gold nanoparticles prepared at addition IPA amounts of (a) 0, (b) 0.05, (c) 0.1, (d) 0.15 and (e) 0.2 mL, respectively. The particles were spherical and the smallest among all the samples when they were prepared without adding IPA, as shown in Fig. 2a. Furthermore, the shape of the particles changed from spherical to elongate rods as the level of IPA increased, as shown in Figs. 2b–2d. The particles tended to be elongated with 0.2 mL of IPA, as depicted in Fig. 2e. The shape of the elongated rods was similar to that of crooked nanorods, as shown in Fig. 2f. Fig. 3 shows the average diameter (d_{average}), average lengths (l_{average}) and standard deviation (σ) of CGNRs. Statistical counting of over 200 particles reveals that the average diameters of CGNRs with 0, 0.05, 0.1, 0.15 and 0.2 mL IPA were the 15.3 ± 3.8, 29.4 ± 10.4, 31.8 ± 12.1, 35.4 ± 13.5 and 35.9 ± 10.2 nm, respectively, as shown in Fig. 3a. Additionally, the average lengths of CGNRs in 0, 0.05, 0.1, 0.15 and 0.2 mL IPA were 15.8 ± 4.6, 31.2 ± 11.1, 40.5 ± 15.6, 45.6 ± 17.9 and 52.3 ± 18.3, respectively, as shown in Fig. 3b. Furthermore, the aspect ratios (γ) for CGNRs were 1.03, 1.06, 1.27, 1.28 and 1.46 nm, respectively; where γ is defined as the ratio of the average length to the average diameter of a cylinder. The γ was found to increase with increasing IPA, clearly indicating that the diameter of CGNRs did not change substantially, whereas the length increased significantly. The surface plasmon absorption changed significantly when the nanoparticle shape was changed [24,25]. Fig. 4a illustrates the formation of a gold network with high IPA (0.5 mL). The gold network was observed over a very long range, and can be described as cross-jointed chains.

3.3. Structures of gold networks

Fig. 4 shows typical TEM images of gold networks prepared with 0.5 mL IPA. The gold networks had a large surface area of several square micrometers, as shown in Fig. 4a. The self-assembled network structure was obtained by connecting

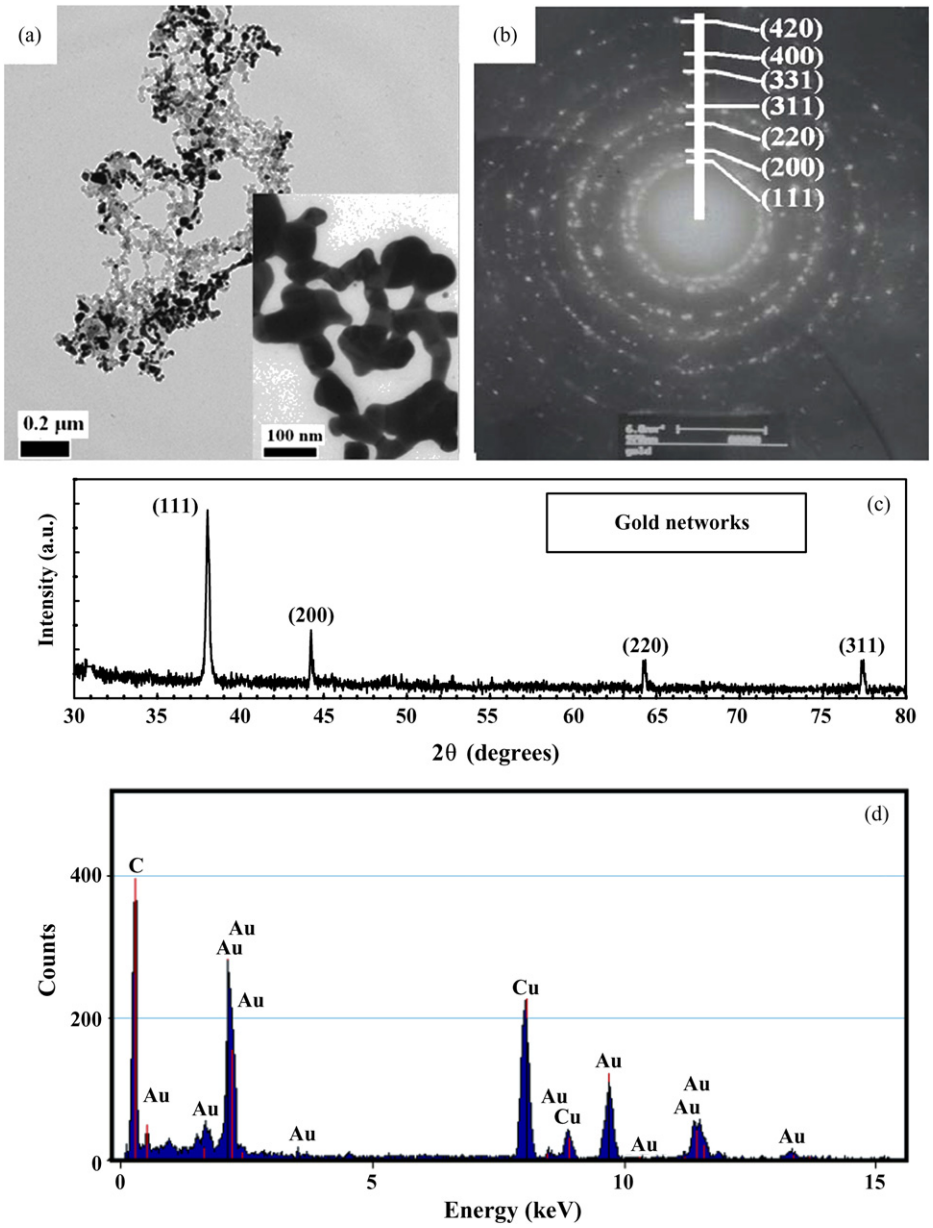

Fig. 4. (a) TEM micrographs of gold networks prepared with 0.5 mL IPA, and magnified image in inset (a). (b) The selected-area electron diffraction pattern of (a). (c) XRD patterns of network structures deposited on quartz substrate. (d) Energy dispersive X-ray spectrum of gold network structure.

several CGNRs of 30 nm in width each other, as shown in the inset of Fig. 4a. The CGNRs, which were very well packed, played a bridging role in the network, linking the other particles. The SAED pattern clearly shows that gold networks are polycrystalline, as shown in Fig. 4b. The SAED pattern of the gold networks was similar to the SAED pattern of CGNRs, but structures of the gold network were more strong crystalline than those of CGNRs. Fig. 4c shows that the XRD pattern for gold network clearly reveals four peaks at 2θ values of 38.18°, 44.39°, 64.57° and 77.54° in this diffraction pattern due to the (111), (200), (220) and (311) Bragg reflections. These results indicate that gold networks had higher anisotropic growth in shape and structure than those of the CGNRs. Furthermore, the samples of the gold networks were confirmed by EDS to be pure gold, as shown in Fig. 4d. No other element was detected by EDS analysis, indicating that these network structures are purely gold.

3.4. Absorption spectrum of crooked gold nanorods and gold networks

The absorption spectra of metallic nanoparticles are well known to depend markedly on the particle shape. Fig. 5 shows the UV–vis absorption spectra of CGNRs with different amounts of IPA. The surface plasmon resonance (SPR) band of CGNRs exhibited a red shift with increasing IPA. Such changes in the SPR bands can be related to those predicted at various γ values. Fig. 6a shows an apparent increase in the aspect ratios and position of SPR band when the IPA level is increased from 0.05 to 0.2 mL. However, the CGNRs with high aspect ra-

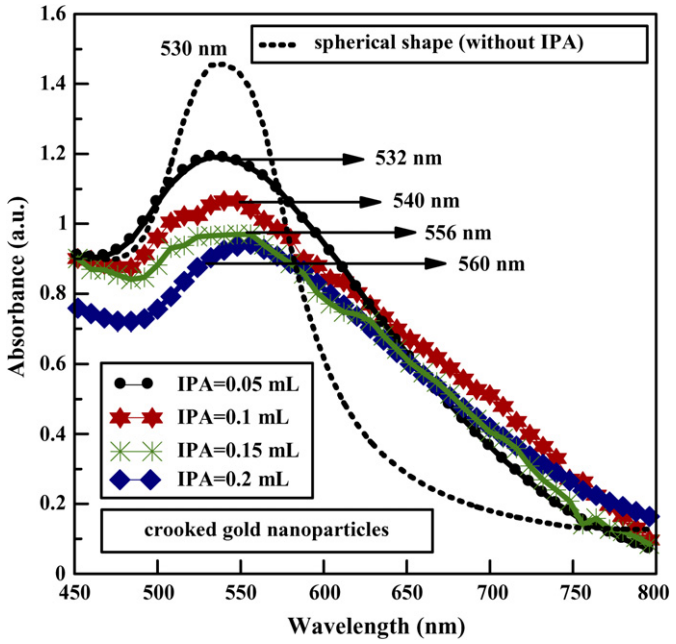

Fig. 5. Absorption spectra of crooked gold nanoparticles prepared with addition of 0.05, 0.1, 0.15, and 0.2 mL IPA.

tios (about 1.46) and SPR bands with long wavelengths (about 560 nm) were obtained by controlling the amount of IPA. The absorption spectrum of CGNRs can be approximately rationalized by analogous absorption behavior of gold nanoprolate particles.

Based on the model calculation, the interaction between the incident electromagnetic wave and a non-spherical metal nanoparticle can be described by the radiation of a lossy dipole induced at the center of the particle. Assuming that the scattering was negligible, the mean absorption cross-section (Q_{abs}) of a nanoprolate particle, averaged over all orientations, was calculated in the dipole approximation as follows [9,18,26]:

$$Q_{\text{abs}} = -\left(8\pi^2/3\lambda\right) \times \ln(\alpha_{\text{l}} + 2\alpha_{\text{t}}),$$

where λ denotes the wavelength of the light in the media, and α_{l} and α_{t} are the levels of polarizability of the spheroid along the longitudinal and transverse axes, respectively. The values of α_{l} and α_{t} are calculated under the assumption that the size dependent dielectric constant of the nanoprolate particle can be treated separately, using the formula

$$\alpha_{\text{l,t}} = V(\varepsilon_{\text{l,t}} - 1)/\left[4\pi + (\varepsilon_{\text{l,t}} - 1)P_{\text{l,t}}\right],$$

where V is the volume of the spheroid whose aspect ratios is γ ($\gamma > 1$); $\varepsilon_{\text{l,t}}$ is the frequency-dependent complex dielectric constant of the particle, and $P_{\text{l,t}}$ are the depolarization factors

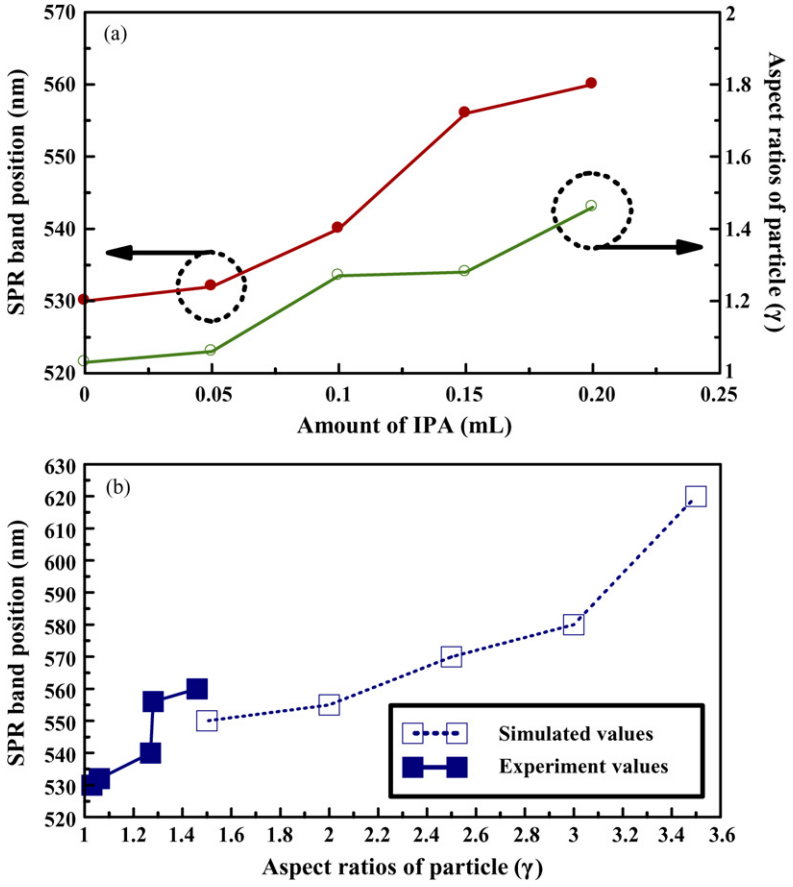

Fig. 6. (a) Maximum position of surface plasmon resonance (SPR) (dark circles) and aspect ratios (γ) of particles (open circles) as functions of the amount of IPA. (b) Maximum position of surface plasmon band using simulated values (open squares) and experiment values (dark squares) as a function of the aspect ratios (γ) of particle.

for the longitudinal and transverse components [27], given by

$$P_l = \left[4\pi/\left(1-\gamma^2\right)\right] \times \left\{\left[\gamma/\left(\gamma^2-1\right)^{1/2}\right]\ln\left[\gamma-\left(\gamma^2-1\right)^{1/2}\right]+1\right\},$$

$$P_t = (4\pi - P_l)/2.$$

The above simulated absorption spectra from equations [28] indicate that the transverse SPR band is damped and becomes insignificant compared to the longitudinal SPR band, and that the longitudinal SPR centered at 570 nm corresponds to a γ value of 2.5. Theoretically $\gamma = 3.5$ corresponds to a high shift in the longitudinal SPR band (620 nm), as shown in simulated values (open squares) of Fig. 6b. In the studies shown in experiment values (dark squares) of Fig. 6b, the shape of particle was almost spherical at an IPA of 0.05 mL, with longitudinal centered SPR and γ values of 532 nm and 1.06, respectively. Furthermore, $\gamma = 1.46$ was obtained in the TEM imagery analysis of the skeleton of longer crooked nanorods (see Fig. 2e), corresponding to a longitudinal SPR centered at 560 nm. Notably, longitudinal SPR bands shifted to long wavelength as the particle aspect ratio increased, as shown in Fig. 6b. Such behavior has been observed in other literatures [29–32].

Fig. 7 shows UV–vis absorption spectrum of gold networks prepared at 0.5 mL IPA, revealing that almost-flat absorbance curves of networks structure were observed at 500–1100 nm, as shown in curve (c) of Fig. 7. Furthermore, the intensity of SPR band increased when the particle shape changed from a network structure to spherical shape. The absorbance of gold networks exhibited a broader peak than that of the spherical and crooked nanorod shape, which displayed an absorbance of long range from the visible to near-infrared ray region. The absorption property of the film of gold in nanoscaled thickness and layer of gold nanoparticles aggregation are analogous to the gold network structures. However, the phenomenon of absorbance band broadening with gold networks structure, as observed in this study, is thus consistent with the literature [33,34].

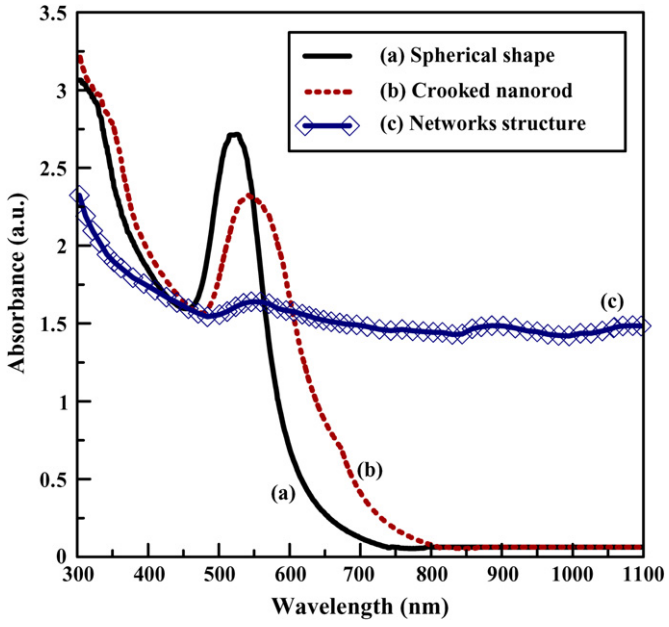

Fig. 7. UV–vis absorption spectra of gold nanoparticles obtained with shape of (a) spherical, (b) crooked nanorod and (c) networks, respectively.

3.5. Proposed formation mechanisms of crooked nanorods and network structures

During the electrochemical process, the bulk metal at the anode is oxidized to metal cations which then migrate to the cathode where reduction reaction occurs with the formation of ad-atoms [35]. These ad-atoms are trapped by the surfactant to form the nanoparticle. The cationic surfactant in this study was based on the nitrogen (N) atom carrying the cationic charge, thus absorbing strongly onto most solid surface, as shown in Fig. 8. The surfactant, the electrolyte and a stabilizer in the growth solution, is generally considered to be a micelle-template to control the particle size and shape. However, all the above results show that the synthesis by micelle-template of surfactant with the addition of IPA solvent is a key step for formation of crooked nanorods, and network structures. Previous studies reveal that surfactant forms a bilayer on the nanoparticle surface as micelle-templates [36]. The presence of the surfactant molecule determined the controlling size and shape of particles, and smaller aggregations were formed as the van der Waals interactions between particles decreased, indicating

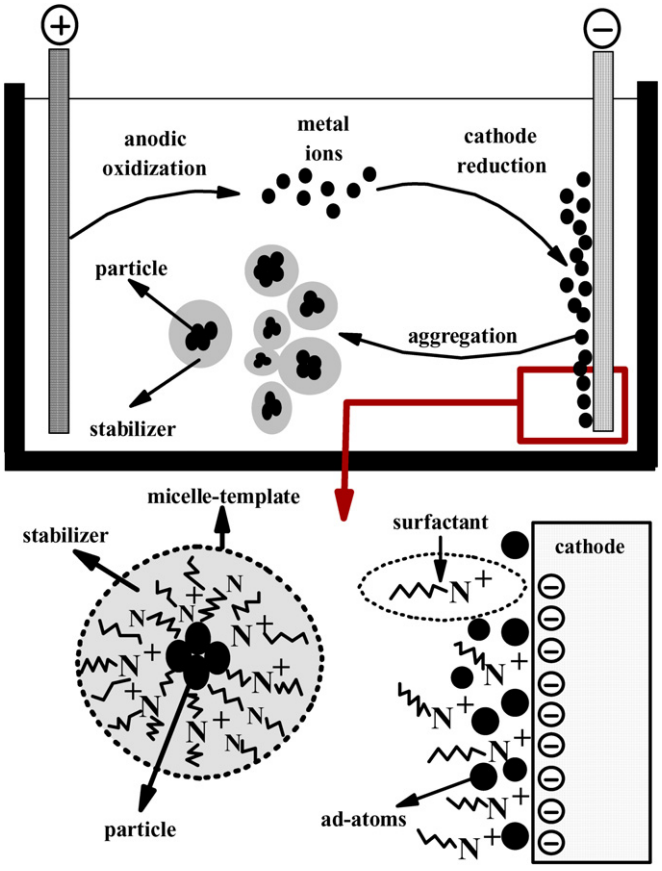

Fig. 8. Schematic diagram of the electrochemical apparatus for gold nanoparticle synthesis. The bulk metal is oxidized at the anode, the metal cationics migrate to the cathode, and reduction occurs with formation of ad-atoms in the zero oxidation state. The surfactant traps these ad-atoms, forming nanoparticles.

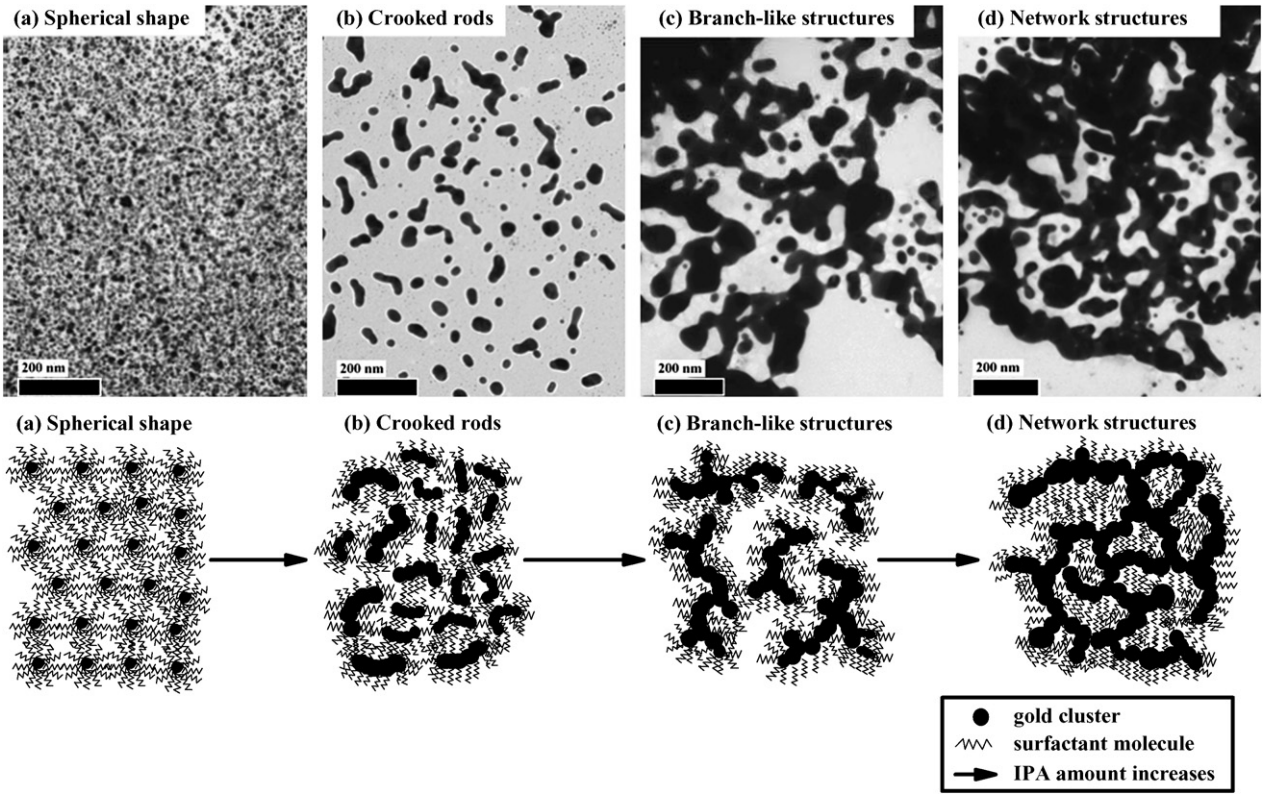

Fig. 9. Schematic illustration of the electrochemical formation of gold network structures with surfactant micelle-templates and addition of IPA solvent (below). The corresponding TEM images analysis (top).

a uniform dispersion for particles. When the organic solvents of alcohols or amines were added with surfactant solution, they could usually dissolve polar surfactant groups at the hydrocarbon/water interface of the micelle, and therefore decreased the surface charge density of the ionic micelles, promoting the formation of micelle-template geometries with low mean curvature, such as rods and discs [37]. Therefore, the lower level of IPA addition caused the micelle-template shape to change, producing crooked nanorod structures. Thus, the hypothesis for the formation of CGNRs can be explained as follows, First, damaging surfactant micelles-template by adding IPA solvent leads to particles with non-uniform size, i.e., formation of large size gold grains and small size gold nuclei or gold ad-atoms during electrochemical growth, as shown in Fig. 2. Second, those small gold nuclei or gold ad-atoms in such an unstable state show a tendency to undergo fusion into surface of large gold grains by the van der Waals attractions forces, and are large enough to favor the aggregation of clusters, indicating that small gold nuclei link the large gold grains to form the crooked nanorod structures, as shown in the inset of Fig. 1e. Yonezawa et al. also reported that unstable gold particles with a size of about 2.7 nm automatically fused into larger particles to form wire-like structures [38]. Therefore, these gold ad-atoms or small size gold nuclei may act as seeds for growth of CGNRs. Furthermore, the formation of interconnected network structures can be explained as follows. Many CGNRs were formed at low IPA levels. The shape of the surfactant micelles-template was acutely damaged at high IPA levels, producing particles of non-uniform size including small nuclei, ad-atoms and CGNRs in growth solution as the precursors. Moreover, the subsequent anisotropic coalescence and aggregation of these precursors led to the formation of an interconnected network structure, as shown in Fig. 9. Hence, adding IPA solvent to a surfactant solution affects the shape of the surfactant micelle-templates, CGNRs formation and the network structure due to the van der Waals attractions force, which favors the formation of special structures.

4. Conclusions

In summary, this study demonstrates the preparation of CGNRs and gold network structures with surfactant micelle-template with addition of isopropanol by an electrochemical technique. The CGNRs had many γ values, and surface plasmon absorption was red-shifted from 532 to 560 nm. The CGNRs were formed from many small gold nuclei aggregation between the large grains during the growth process, indicating that small gold nuclei linked the large gold grains. The gold network structure was obtained by interconnecting several CGNRs to form the interconnected network structures, which were observed with the almost-flat absorbance curves and broad peaks from 500 to 1100 nm. Various characterizations such as UV–vis absorption spectrum, TEM, SEAD and XRD show that the resultant gold nanoparticles had good and stable characteristics. This work indicates that the electrochemical method is suitable for low-cost, low-temperature and rapid fabrication of gold nanoparticles.

Acknowledgments

This work was partially supported by the National Science Council (NSC) of the Republic of China under Contract No. 92-2215-E-218-003. The authors gratefully acknowledge the Department of Mechanical Engineering, Southern Taiwan University of Technology in Taiwan for high-resolution TEM, EDS, SEAD, and XRD measurements.

References

[1] G.T. Wei, F.K. Liu, C.R.C. Wang, Anal. Chem. 71 (1999) 2085.
[2] C.A. Foss, G.L. Hornyak, J.A. Stockert, C.R. Martin, J. Phys. Chem. 96 (1992) 7497.
[3] Y. Sun, B. Gates, B. Mayers, Y. Xia, Nano Lett. 2 (2002) 165.
[4] F. Kim, J.H. Song, P. Yang, J. Am. Chem. Soc. 124 (2002) 14316.
[5] J. Gao, C.M. Bender, C.J. Murphy, Langmuir 19 (2003) 9065.
[6] Y.J. Zhu, X.L. Hu, Chem. Lett. 32 (2003) 1140.
[7] T. Reuter, O. Vidoni, V. Torma, G. Schmid, Nano Lett. 2 (2002) 709.
[8] F. Mafuné, J. Kohno, Y. Takeda, T. Kondow, J. Phys. Chem. B 107 (2003) 12589.
[9] C.D. Chen, Y.T. Yeh, C.R.C. Wang, J. Phys. Chem. Solids 62 (2001) 1587.
[10] J.Y. Chang, J.J. Chang, B. Lo, S. Tzing, Y. Lin, Chem. Phys. Lett. 379 (2003) 261.
[11] I. Lisiecki, F. Billoudet, M.P. Pileni, J. Phys. Chem. 100 (1996) 4160.
[12] Q. Lu, F. Gao, S. Komarneni, J. Am. Chem. Soc. 126 (2004) 54.
[13] B. Liu, H.C. Zeng, J. Am. Chem. Soc. 126 (2004) 8124.
[14] S. Pang, T. Kondo, T. Kawai, Chem. Mater. 17 (2005) 3636.
[15] A. Chen, X. Peng, K. Koczkur, B. Miller, Chem. Commun. (2004) 1964.
[16] M.T. Reetz, W. Helbig, J. Am. Chem. Soc. 116 (1994) 7401.
[17] B. Yin, H. Ma, S. Wang, S. Chen, J. Phys. Chem. B 107 (2003) 8898.
[18] Y.Y. Yu, S.S. Chang, C.L. Lee, C.R.C. Wang, J. Phys. Chem. B 101 (1997) 6661.
[19] S.S. Chang, C.W. Shih, C.C. Chen, W.C. Lai, C.R.C. Wang, Langmuir 15 (1999) 701.
[20] C.J. Huang, Y.H. Wang, P.H. Chiu, M.C. Shih, T.H. Meen, Mater. Lett. 60 (2006) 1896.
[21] C.J. Huang, P.H. Chiu, Y.H. Wang, M.C. Shih, T.H. Meen, J. Electrochem. Soc. 153 (2006) D129.
[22] C. Pascal, J.L. Pascal, F. Favier, Chem. Mater. 11 (1999) 141.
[23] C.H. Kuo, T.F. Chiang, L.J. Chen, M.H. Huang, Langmuir 20 (2004) 7820.
[24] U. Kreibig, M. Vollmer, Optical Properties of Metal Clusters, Springer-Verlag, Berlin, 1995.
[25] M.B. Mohamed, S. Link, M.A. El-Sayed, J. Phys. Chem. B 102 (1998) 9370.
[26] M. Kerker, The Scattering of Light and Other Electromagnetic Radiation, Academic Press, New York, 1969.
[27] J.A. Creighton, D.G. Eadon, J. Chem. Soc. Faraday Trans. 87 (1991) 3881.
[28] I. Lisiecki, F. Billoudet, M.P. Pileni, J. Phys. Chem. 100 (1996) 4160.
[29] E.J. Zeman, G.C. Schatz, J. Phys. Chem. 91 (1987) 634.
[30] M.P. Cline, P.W. Barber, R.K. Chang, J. Opt. Soc. Am. B 3 (1986) 15.
[31] L. Pei, K. Mori, M. Adachi, Chem. Lett. 33 (2004) 324.
[32] C.J. Huang, Y.H. Wang, P.H. Chiu, J.J. Lin, Chem. Lett. 35 (2006) 30.
[33] T. Baun, D. Bethell, D.J. Schiffrin, Langmuir 15 (1999) 866.
[34] M.D. Musick, D.J. Pena, S.L. Botsko, T.M. McEvoy, J.N. Richardson, M.J. Natan, Langmuir 15 (1999) 844.
[35] M.T. Reetz, M. Winter, R. Breinbaur, T.T. Albrecht, W. Vogel, J. Chem. Eur. 7 (2001) 1084.
[36] B. Nikoobakht, M.A. El-Sayed, Langmuir 17 (2001) 6368.
[37] M. Tornblom, U. Henriksson, J. Phys. Chem. B 101 (1997) 6028.
[38] T. Yonezawa, S. Onoue, N. Kimizuka, Chem. Lett. 12 (2002) 1172.